Cavity sub- and superradiance for transversely driven atomic ensembles

Christoph Hotter, Laurin Ostermann ⬤, and Helmut Ritsch ⬤

Institut für Theoretische Physik, Universität Innsbruck, Technikerstr. 21a, A-6020 Innsbruck, Austria

Large atomic ensembles coupled to a single optical resonator mode can be steered to strongly enhanced or suppressed collective emission via phase controlled excitation. Employing the Tavis-Cummings model we find so far unreported phenomena. Using a second order cumulant expansion we predict that a homogeneously excited ensemble equally distributed between odd and even sites along the cavity mode is extremely subradiant as long as the average excitation remains below 50%, but shows pulsed emission for inversion. The combination of these two properties enables the implementation of an efficient cavity-enhanced Ramsey probing featuring a fast readout and minimal heating with particular advantages for atomic clock transitions. For continuous illumination the nonlinear atom-field interaction induces regular superradiant self-pulsing. Additionally, we observe an increased pulse delay time in comparison to an excitation through the cavity.

I. INTRODUCTION

The phenomena of super- and subradiance originating from constructive or destructive interference of the field radiated by an ensemble of dipoles has been studied for many decades [1–10]. The decisive quantity is the collective dipole moment of the emitters with respect to the system's electromagnetic radiation modes which, apart from the ensemble's quantum state determining the internal phase relations, is strongly tied to their spatial distribution. For superradiance, phase coherence in one given emission mode is sufficient, yet, subradiance only appears when virtually all of the emission channels are blocked by destructive interference. While there are classical analogs of super- and subradiance, in quantum emitters the radiation is triggered by local vacuum fluctuations of the electromagnetic field, which are determined by the system's geometry [11–13]. These are isotropic and homogeneous in free space, but can be modified by, e.g., placing them in the evanescent field of a waveguide [9,14,15], inside a hollow core photonic crystal fiber [16], engineering interactions for superconducting qubits [17], or as in our case putting them inside a (linear) resonator, which yields more precise control over their interference.

Pulsed superradiant output has been demonstrated for large atomic ensembles in optical cavities [8,18–20]. Superradiant lasing [21–23] is one of the prime applications of cavity superradiance and even self-organization [24] can incorporate superradiant behavior. In contrast, subradiance is a lot harder to access experimentally [25] and treat theoretically [10,26,27].

In order to induce cavity mediated superradiant light emission from an atomic ensemble, it is favorable to excite the atoms through the cavity instead of from the side, since in this case all atoms obtain the same relative phase with respect to the cavity mode to constructively emit photons into the cavity [8,28]. This raises the question about the behavior of an ensemble with arbitrary or vanishing relative phases, as it is, e.g., naturally the case for a transversely driven large atomic ensemble, homogeneously distributed along the cavity axis covering odd and even sites of the cavity mode. On the one hand, one could intuitively think that an ensemble with vanishing relative phase features a subradiant behavior, since the light emitted into the cavity interferes destructively [24]. But, on the other hand, there is no phase information stored in a fully excited ensemble, hence, the dynamics of atoms inverted through the cavity or from the side must be
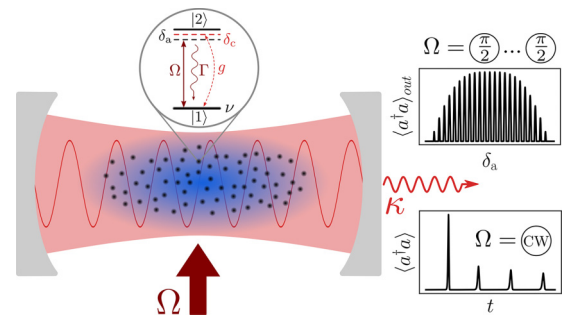

FIG. 1. Cavity Sub- and Superradiance Model. We consider a homogeneous, dilute ensemble of narrow line two-level atoms at random but fixed positions in a standing wave optical resonator coherently driven by a transverse plane wave laser. We assume a weak single atom but strong collective coupling regime, i.e., $\kappa, \sum_j g_j^2/\kappa \gg \Gamma \gg g_j^2/\kappa$. The cavity Ramsey fringes and the photon number self-pulsing are indicated as cavity output signals for the respective drive laser operations.

identical in this case, i.e., the emission of a superradiant pulse [8,17–20].

In this paper we show that there is a transition between cavity super- and subradiance for an atomic ensemble with vanishing relative phase. In particular, an inverted ensemble emits a superradiant pulse, whereas a noninverted ensemble features a subradiant behavior. This can be crucial for the understanding and design of cavity QED experiments. Utilizing this transition from cavity sub- to superradiance enables the implementation of a cavity-enhanced Ramsey spectroscopy. The central idea is that the noninverted ensemble is decoupled from the cavity during the free evolution phase [29,30], but the final readout of the inverted atoms is still performed via the superradiant manifold. This scheme allows for a fast and precise readout, without destroying the measured ensemble. Beyond that, we find a yet unreported self-pulsing of the cavity output field upon continuously driving the ensemble, which can be explained by the system dynamics cyclically transitioning from cavity subradiance to superradiance. Lastly, our setup can be employed to more accessibly measure delay time statistics, when pumping the ensemble transversally instead of through the cavity as the cavity subradiance in this case will slow down the system's dynamics, making the output easier to detect.

II. MODEL

We consider N two-level atoms with a narrow transition at frequency ω_a coupled to a single mode cavity. The atoms are coherently driven with a detuning between the laser and the atomic transition of $\delta_a = \omega_l - \omega_a$, the corresponding Rabi frequency is denoted by Ω. The cavity is detuned by $\delta_c = \omega_l - \omega_c$ from the laser and we have an atom-cavity coupling of g_j for the j-th atom. The system is depicted in Fig. 1. Its Hamiltonian in the rotating frame of the pump laser reads

$$
H = -\delta_c a^\dagger a + \sum_{j=1}^{N} \Bigg[-\delta_a \sigma_j^{22}
$$

$$
+ g_j \big(a^\dagger \sigma_j^{12} + a\sigma_j^{21}\big) + \frac{\Omega}{2}\big(\sigma_j^{21} + \sigma_j^{12}\big) \Bigg], \qquad (1)
$$

with the cavity photon creation (annihilation) operator $a^\dagger$ (a) and the atomic transition operator $\sigma_j^{kl} = |k\rangle_j \langle l|_j$ for the j-th atom. The coherent interaction is accompanied by dissipative processes accounted for by the Liouvillian $\mathcal{L}[\rho]$ in the master equation

$$
\dot{\rho} = i[\rho, H] + \mathcal{L}[\rho]. \qquad (2)
$$

In the Born-Markov approximation [31] we can write the Liouvillian in Lindblad form as

$$
\mathcal{L}[\rho] = \sum_i R_i (2J_i \rho J_i^\dagger - J_i^\dagger J_i \rho - \rho J_i^\dagger J_i), \qquad (3)
$$

with the jump operators $\{J_i\}$ and their corresponding rates $\{R_i\}$ shown in Table I, including cavity photon losses as well as individual decay and dephasing of the atoms.

As we are targeting narrow clock transitions the system is operated in the bad and large volume cavity regime $\kappa \gg \Gamma$ with only a small single atom cooperativity $C_j = g_j^2/(\kappa \Gamma) \ll$

TABLE I. Dissipative Processes. The system features a damped cavity mode as well as atomic decay and dephasing.

i	J_i	R_i	Description
1	a	κ	cavity photon losses
2	σ_j^{12}	Γ	decay from $|2\rangle_j$ to $|1\rangle_j$
3	σ_j^{22}	ν	dephasing of the j-th atom

1 but a sufficiently large ensemble to enter the strong collective coupling regime $NC = \sum_j C_j \gg 1$. Typically, this parameter regime implies a very large atom number, which does not allow for a full quantum simulation, but we can very well treat this problem in a second order cumulant expansion [32,33]. A comparison with a full quantum simulation for a small atomic ensemble is shown in Appendix C. Additionally, we neglect dipole-dipole interaction [4], as our atomic ensemble is sufficiently dilute. This also means that the individual free space decay rate of the atoms is not affected.

Throughout the paper we calculate the dynamics in a second order cumulant expansion [33,34]. Nevertheless, the mean-field equations already contain the key physics and therefore we present these much simpler equations for a qualitative description of the system:

$$
\frac{d}{dt}\langle a\rangle = -\left(i\delta_c + \frac{\kappa}{2}\right)\langle a\rangle - i\sum_{j=1}^{N} g_j\langle\sigma_j^{12}\rangle, \qquad (4a)
$$

$$
\frac{d}{dt}\langle\sigma_j^{22}\rangle = -\Gamma\langle\sigma_j^{22}\rangle + i\frac{\Omega}{2}\big[\langle\sigma_j^{12}\rangle - \langle\sigma_j^{21}\rangle\big]
$$

$$
+ ig_j\big[\langle a^\dagger\rangle\langle\sigma_j^{12}\rangle - \langle a\rangle\langle\sigma_j^{21}\rangle\big], \qquad (4b)
$$

$$
\frac{d}{dt}\langle\sigma_j^{12}\rangle = \left(i\delta_a - \frac{\Gamma+\nu}{2}\right)\langle\sigma_j^{12}\rangle
$$

$$
+ i\left(\frac{\Omega}{2} + g_j\langle a\rangle\right)\big[2\langle\sigma_j^{22}\rangle - 1\big]. \qquad (4c)
$$

III. COLLECTIVE CAVITY MEDIATED SUPER- AND SUBRADIANCE

In the following, for simplicity, we assume the atoms located close to cavity mode antinodes with half of the atoms at the maxima and half at the minima of the mode function along the cavity axis. Hence their respective effective coupling is well approximated by $+g$ and $-g$. As confirmed by more involved simulations, investigating a random distribution for the atom-field coupling, this simplification already captures the essential physics.

Inverting all atoms with a short π-pulse induces the emission of a delayed intense light pulse due to cavity-enhanced superradiant decay [8,17–20]. Synchronized stimulated emission in a cavity occurs even for a dilute ensemble, which does not exhibit free space superradiance. Figure 2(a) shows typical trajectories for the corresponding time evolution of the intracavity photon number $\langle a^\dagger a\rangle$. When all atoms are initially coherently prepared at $\langle\sigma^{22}\rangle = 80\%$ (black line), a superradiant pulse emerges. Figure 2(b) depicts the corresponding time evolution of the excited state population, showing the cavity
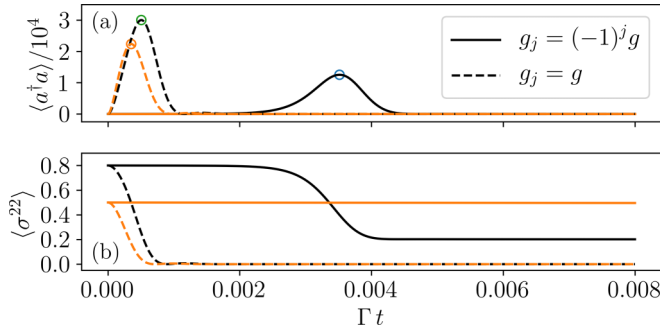
FIG. 2. Cavity Mediated Collective Decay. Time evolution of the intracavity photon number (a) and the single atom excited state population (b) after a short pulse excitation preparing each atom in the same coherent superposition. The black line represents an inverted ensemble with $\langle\sigma^{22}\rangle = 80\%$ excited state fraction ($\approx 3\pi/4$-pulse) and the orange line depicts an ensemble after a $\pi/2$-pulse to create $\langle\sigma^{22}\rangle = 50\%$. For uniform cavity coupling (dashed line) we see an immediate superradiant population decay to the ground state creating a photon pulse in the cavity. Cavity coupling with alternating signs (solid line) leads to a weaker and time delayed pulse for an inverted ensemble, while the atomic excitation is almost perfectly protected from cavity decay without inversion [solid line in (b)]. We have assumed $N = 2 \cdot 10^5$ atoms with $g = 10\Gamma$, $\kappa = 10^4\Gamma$, and $\delta_a = \delta_c = \nu = 0$.

mediated decay of the atoms. For comparison we display the behavior for all atoms equally coupled to the cavity (dashed line, $g_j = g$), similar to the case of excitation through the cavity [8,28], showing a much faster and stronger pulse.

However, for the system we consider with alternating coupling ($g_j = (-1)^j g$), the dynamics depend drastically on the population of the atoms. Interestingly, we observe such pulsed emission for an ensemble of inverted atoms only. If the excited state population is below 50% the atoms do not emit a significant amount of photons into the cavity mode, see solid orange line in Fig. 2. Figure 3(a) shows the total number of emitted photons $\langle a^\dagger a \rangle_{\text{out}}$ for different values of the initial excited state population. Almost no photons leak through the cavity mirrors until the atoms are inverted. Again, the dashed line represents the case of all atoms coupling equally ($g_j = g$), resembling a pulsed excitation of the atoms through the cavity. We see that also noninverted atoms superradiantly emit photons into the cavity mode without retaining excitation. Additionally, we plot the peak intracavity photon number (blue) demonstrating the same behavior.

Figure 3(b) shows the average delay time of the peak photon number as a function of the atomic excitation. For uniformly coupled atoms (dashed line) a higher excitation leads to a later pulse. Whereas for alternating coupling (solid line) the delay time of the peak increases for lower inversion and is larger in general. For a perfect π-pulse excitation both cases lead to identical superradiant pulses in terms of delay time as well as photon number, since for fully inverted atoms the phase of the coupling does not matter. However, for only slightly imperfect π-pulses one already obtains much longer delay times for a transversely excited ensemble, than for an excitation through the cavity. Several experimental setups should allow for observing this result [8,18–20,28].
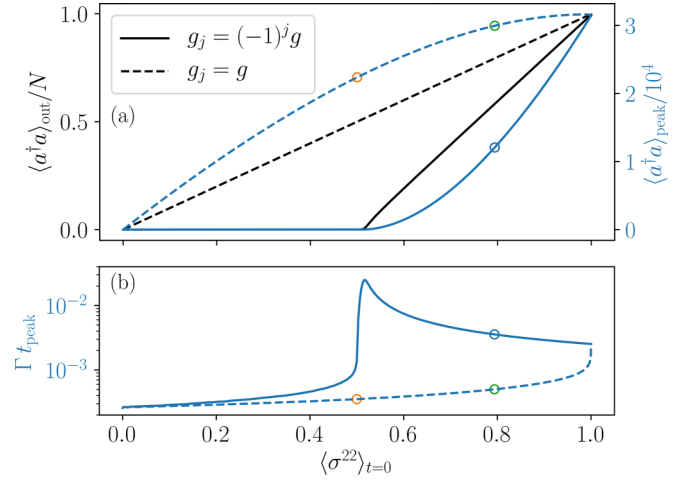

FIG. 3. Cavity Sub- and Superradiance. (a) Comparison of the cavity-output photon number $\langle a^\dagger a \rangle_{\text{out}} = \kappa \int \langle a^\dagger a \rangle \mathrm{d}t$ (black) and peak intracavity photon number (blue) as a function of the single atom excitation probability for alternating coupling (solid line) and uniform coupling (dashed line). Note the strong suppression of superradiant emission in the alternating coupling case as long as no inversion is created initially. (b) Delay time of the peak photon number. For alternating coupling the pulse appears later in general and is more delayed for decreasing inversion, whereas for equally coupled atoms the pulse delay time increases with growing excited state population. The circles indicate the parameters chosen for Fig. 2(a).

The origin of this subradiant suppression for a noninverted ensemble is the destructive interference [5–7,29] of photons emitted by the atoms coupled to the cavity with opposite g, in contrast to the widely studied synchronized superradiant emission due to constructive interference for a large inverted ensemble [8,18–20,28]. Analyzing the mean-field Eqs. (4a) to (4c) explains the transition between cavity sub- and superradiance qualitatively. First, from Eq. (4a) we notice the significance of the alternating coupling: the cumulative dipole moment of the atoms projected on the cavity mode $\sum_j g_j \langle \sigma_j^{12} \rangle$ vanishes [29,30] and hence the gain in the cavity field disappears. For simplicity we have chosen the same laser excitation phase for all atoms. Yet a varying excitation phase works equally well as long as the overall relative phase disappears. Typically, this is implicitly realized in a random spatial distribution of a sufficiently large and dilute ensemble. It is also true for a ring cavity featuring a continuous atom-cavity coupling phase along the cavity axis [24] or for atoms coupled to waveguides or inside hollow core fibers with appropriate spacing [9,14–16]. Furthermore, we see why an excitation through the cavity is effectively the same as all atoms equally coupled and excited from the side: with a drive through the cavity the phase of the coherence $\langle \sigma_j^{12} \rangle$ is determined by the phase of the coupling g_j, therefore the individual parts of the sum in Eq. (4a) all carry the same phase and do not compensate.

By these arguments only there seems to be no difference in the behavior of inverted and noninverted atoms, since the sum in Eq. (4a) does not depend on the excited state population. Therefore we calculate the second time derivative of the cavity field to obtain a qualitative description. By inserting Eq. (4c)

with $\langle \sigma_j^z \rangle = 2\langle \sigma_j^{22} \rangle - 1$ we find

$$\frac{d^2}{dt^2} \langle a \rangle = \sum_j g_j^2 \langle \sigma_j^z \rangle \langle a \rangle + \underbrace{[\ldots]}_{\text{decay}}. \tag{5}$$

For a clear view we set $\delta_a = \delta_c = 0$ and hint at the dissipative processes only. For short times, i.e., $\langle \sigma_j^z \rangle$ is constant, a nonzero initial field $\langle a \rangle_{t=0} \neq 0$ leads to the following possible solutions of Eq. (5): for inverted atoms ($\langle \sigma_j^z \rangle > 0$) the field increases rapidly as a cosh function, which leads to the build up of the photon pulse, whereas for noninverted atoms ($\langle \sigma_j^z \rangle < 0$) the field oscillates between zero and the initial value and is strongly damped due to the large cavity decay rate. Having to require a nonzero initial field is an artifact of the mean-field treatment in order to obtain a nontrivial solution and becomes unnecessary for higher order descriptions.

A. Dicke States Representation

In the mean field approximation the total number of output photons for a noninverted atomic ensemble with vanishing cumulative dipole moment is exactly zero. However, a closer investigation in second order cumulant expansion shows that there actually is a small amount of photons released into the cavity. Another interesting aspect of the system is that an initial inversion with $\langle \sigma^{22} \rangle < 1$ leads to $N \cdot (2\langle \sigma^{22} \rangle - 1)$ photons only, as shown in Fig 3(a). Consequently, the atoms retain an excited state population of $1 - \langle \sigma^{22} \rangle$ after the pulsed photon emission into the cavity, indicated by the solid line in Fig. 2(b). To explain these two features we use the Dicke states [1] of the atomic ensemble, which provide an intuitive picture for our considered system.

An ensemble of N identical two-level atoms can be expressed in the basis of Dicke states $|J, M\rangle$, with

$$J^z |J, M\rangle = \frac{1}{2} \sum_j \sigma_j^z |J, M\rangle = M |J, M\rangle, \tag{6a}$$

$$\vec{J}^2 |J, M\rangle = \frac{3N}{4} + \frac{1}{4} \sum_{j \neq k} \left[\sigma_j^{21} \sigma_k^{12} + \sigma_j^z \sigma_k^z \right] |J, M\rangle$$
$$= J(J+1) |J, M\rangle, \tag{6b}$$

where $|M| \leqslant J$ and $0 \leqslant J \leqslant N/2$ [1,26,35,36]. In this description collective decay has a particularly simple behavior, the J quantum number is unchanged, while M is reduced. In the triangle shaped Dicke state diagram in Fig. 4 this corresponds to a vertical line of decreasing M [26,35,36], where the change in M directly reflects the number of lost excitations (photons).

The collective emission in our system is induced by the cavity, with the crucial feature of alternating coupling. In the representation where the cavity mediated decay is described by a vertical line, this leads to a different distribution of the J quantum number due to the different relative phases between the atoms and the cavity field, see Appendix B. Figure 4 compares the mapping of $N = 40$ identically coupled atoms, where states of maximal J are occupied exclusively, to the case of alternating cavity coupling, where states close to the boundary of minimal J are populated predominantly. Note that one finds very similar distributions for an incoherently
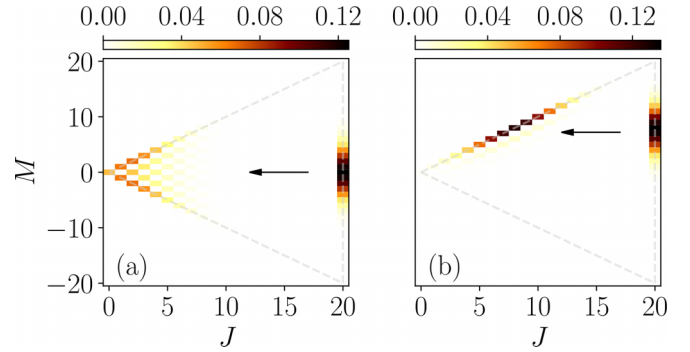

FIG. 4. Dicke States. Population of the Dicke states for $N = 40$ atoms after an initial $\pi/2$-pulse in (a) and $3\pi/4$-pulse in (b). The states occupying the maximal J values correspond to the equally coupled case ($g_j = g$), whereas the states close to the boundary of minimal J represent the alternating coupling case ($g_j = (-1)^j g$). The arrow indicates the mapping between the two cases.

pumped ensemble [26,36]. In this representation we can explain the two features mentioned above in a straight-forward way by recalling that the collective decay decreases M to its minimally possible value $M = -J$ only, without changing J and releasing $|J + M|$ photons. Under collective decay a state $|J, M = +J\rangle$ will thus go to $|J, M = -J\rangle$, explaining the remaining excited state population of $1 - \langle \sigma^{22} \rangle$ after the pulse. Furthermore, we obtain the total number of released photons by summing up the emitted excitations of each state weighted by the corresponding population. This explains the small losses after a coherent $\pi/2$-pulse preparation, see Fig. 4(a). Note that the coherent excitation leads to a binomial distribution in M, regardless of the cavity coupling. Therefore, the width of the distribution per atom becomes narrower as $1/\sqrt{N}$ for an increasing number of atoms. Combined with the feature that the alternating coupling effectively occupies states close to the boundary of minimal J yields a shrinking percentage of lost excitations for a noninverted ensemble for large atom numbers.

B. Atom Number Dependence

So far we have specified the cavity sub- and superradiance qualitatively only. A common way of defining sub- and superradiance quantitatively is the scaling of the emitted light with the atom number [1,3,26]. In our case there are two possibilities to do this: the usual approach is to look at the emitted peak photon number. In Fig. 5(a) and Fig. 5(b) we see that for an inverted ensemble we obtain a large peak photon number proportional to the atom number squared (black dashed line), and for a noninverted ensemble the peak is orders of magnitude smaller and increases less than linearly with the atom number. At the threshold $\langle \sigma^{22} \rangle_{t=0} = 50\%$ it scales linearly with the number of atoms [Fig. 5(b) grey dashed line]. The other way of quantifying sub- and superradiance is the total number of emitted photons through the cavity. In Fig. 5(c) the output photon number scales linearly with the atom number in the superradiant domain and is independent of N in the subradiant regime. Therefore, the number of lost photons per atom reduces for increasing particle numbers in a noninverted ensemble.
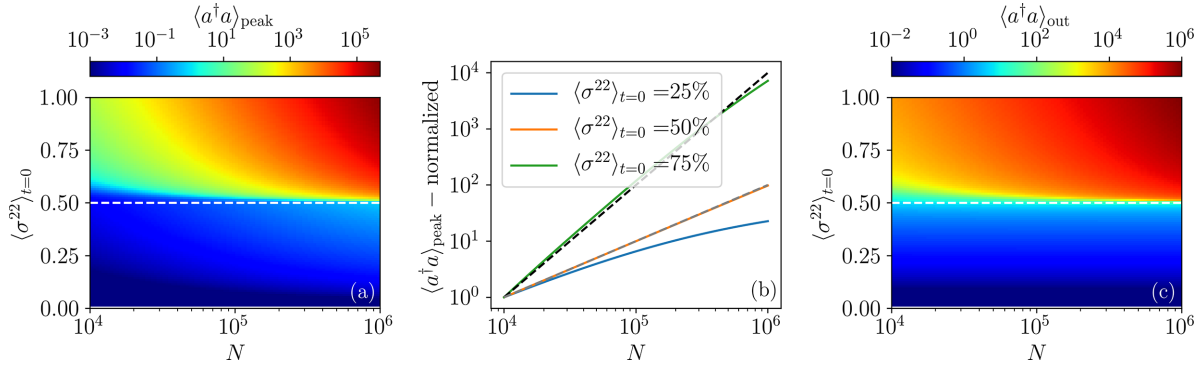
FIG. 5. Atom Number Scaling. Scan of the atom number N and initial excitation $\langle \sigma^{22} \rangle_{t=0}$ for (a) the peak photon number and (c) the output photon number, to quantify and define the cavity sub- and superradiance regions. (b) Shows the peak photon number for three different examples of initial excited state population. The photon number is normalized to the one at $N = 10^4$ for the respective value of $\langle \sigma^{22} \rangle_{t=0}$ to compare the different scalings.

IV. CAVITY-ENHANCED RAMSEY PROBING

The suppression and delay of superradiance for a transverse excitation can be advantageous for storing excitations in an atomic ensemble, however, it might also be undesired if one is interested in fast emission of light. Thus, we can either use it to our advantage or try to avoid it, depending on the intended behavior of the system. For example, it can be convenient to store up to $N/2$ excitations in N two-level atoms in some type of quantum battery [37–39], however, releasing this energy on demand becomes more involved for a transverse excitation. On the other hand, if we strive for fast superradiant emission, as in superradiant lasing [18,19,23,40], a coherent drive along the cavity axis should be preferred due to faster and stronger light emission. In any case, whether suppression of superradiance is desirable or not, it is crucial for the understanding, description, and design of state of the art experiments [8,18–20,28,41].

A particular application we would like to highlight in this section is a cavity-enhanced Ramsey scheme, inspired by Ref. [29], where this idea was first presented for free space atoms. A transverse pump with an overall vanishing phase of the atom-cavity coupling allows for a $\pi/2$-pulse excitation of the atomic ensemble without an immediate rapid superradiant decay through the cavity. Combining this feature with fast direct measurements of the number of excited atoms via the superradiantly emitted cavity photons after the second Ramsey pulse allows for an implementation of a new cavity-assisted Ramsey spectroscopy. The crucial advantage of this scheme is that it can be very fast with no additional manipulation of the atoms needed for the read out, hence the signal is less perturbed. Furthermore, the atoms are not significantly heated by this measurement and can therefore be reused, remarkably reducing the dead time between measurements. Another advantage to other nondestructive measurements for atomic clocks [42–44] is that the signal, i.e., the number of photons, scales linearly with the number of atoms. So, in principle, an arbitrarily large number of atoms can be employed, drastically increasing the signal to noise ratio.

Figure 6(a) shows the output signal, the total number of photons leaking through the cavity mirrors as a function of the laser-atom detuning δ_a. Similar to the conventional Ramsey method, fringes appear [45–47]. One striking difference, however, is that a noninverted ensemble does not produce a signal, corresponding to the flat zero-photon regions. This narrows the FWHM of the cavity Ramsey fringes slightly compared to the conventional Ramsey fringes [see Fig. 6(b)]. Including an atomic dephasing with $\nu = 10\Gamma$ (dashed line) merely weakens the signal, yet, the shape of the curve is essentially the same. By choosing $\delta_c = \delta_a$ we have implicitly assumed that the cavity is perfectly on resonance with the atomic transition. Therefore, one might wonder if a detuned cavity impairs the signal. But, since we operate deeply in the bad cavity regime, only shifts of the cavity resonance frequency on the order of κ are important.

Overall, i.e. that enhancing the Ramsey spectroscopy by adding a cavity achieves the same (or even slightly improved) accuracy, but has the advantage of a convenient, fast, nondestructive measurement scaling linearly in the atom number, which can substantially reduce the measurement dead time. At this point we want to mention that the atoms initially need to be in the ground state for each subsequent measurement. As we saw in Fig. 2(b), a not fully inverted ensemble will retain
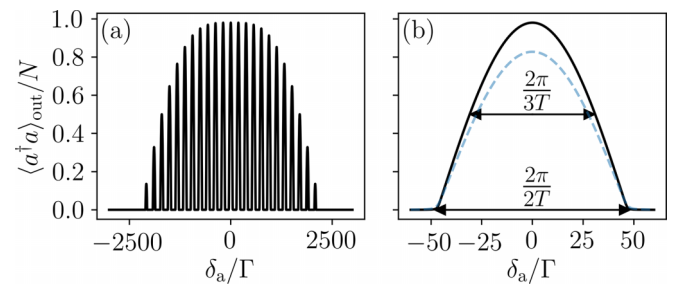

FIG. 6. Cavity Ramsey Method. (a) Fringes in the photon number obtained via the cavity Ramsey method with characteristic flat zero-photon regions. (b) Zoom-in on the central fringe. The FWHM (π/T) of an optimal independent atom Ramsey sequence with waiting time T and the cavity Ramsey fringe ($\sim 2\pi/3T$) are highlighted. The parameters are $N = 2 \cdot 10^5$, $g = 10\Gamma$, $\kappa = 10^4 \Gamma$, $\delta_c = \delta_a$, $\Omega = 1000\Gamma$, and $\nu = 0$ (solid) or $\nu = 10\Gamma$ (dashed). The free evolution time between the two $\pi/2$-pulses is $T = \pi/100\Gamma$. An example cavity Ramsey time evolution is shown in Appendix A.
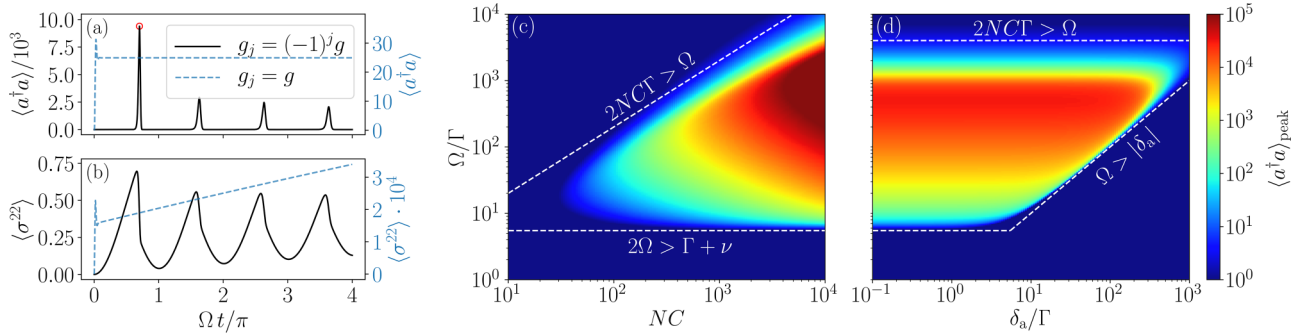
FIG. 7. Self-Pulsing. Time evolution of the cavity photon number (a) and excited state population (b) for a continuous drive, resulting in photon number self-pulsing. (c) and (d) Scans over Ω, NC, and δ_a for the peak photon number of the first pulse [red circle in (a)]. The dashed white lines represent the threshold $2NC\Gamma > \Omega > |\delta_a|$, $(\Gamma + \nu)/2$. The parameters when kept constant are $N = 2 \cdot 10^5$, $g = 10\Gamma$, $\kappa = 10^4\Gamma$, $\delta_c = \delta_a = 0$, $\Omega = 100\Gamma$, and $\nu = 10$.

some population in the excited state. This means one needs to bring these atoms back to the ground state. Unfortunately, this is not possible in a straight-forward way via a coherent drive on the clock transition only. However, there are other ways to achieve this, e.g. with an induced decay via another transition or by depleting the ground state population temporarily to some other level.

Obviously, this cavity-assisted Ramsey procedure will not work for $\pi/2$-pulse excitations through the cavity mirrors as all atoms would exhibit the same relative atom-cavity phase and will therefore already decay superradiantly after the first $\pi/2$-pulse [8,28], corresponding to the case of equal coupling ($g_j = g$) in Fig. 2 and Fig. 4.

V. SELF-PULSING UNDER CONTINUOUS ILLUMINATION

Continuously driving the ensemble with a suitable Rabi frequency leads to striking self-pulsing of the system as shown in Fig. 7(a). Yet, the explanation for this initially surprising behavior is rather simple: as we have seen, the photon emission into the cavity for a noninverted atomic ensemble with vanishing relative phase is strongly suppressed. Therefore, there is no significant cavity photon number at least until $t = \pi/2\Omega$ [see Fig. 7(b)]. But, as soon as a certain population inversion is achieved the ensemble emits a superradiant pulse into the cavity. Subsequently, the excited state population is depleted below 50% and the photon number quickly reduces to almost zero due to the very fast cavity decay. Since the laser is still on, the procedure starts over and we obtain another pulse, i.e., the system dynamically cycles from cavity sub- to superradiance. As we can see in Fig. 7(a) the peak photon number reduces from pulse to pulse. This can be explained in the Dicke state picture, where the not fully inverted ensemble retains some excitation after the collective emission and hence starts over from this instead of the ground state, which leads to less inversion for the next pulse.

Additionally, the time evolution for equally coupled atoms (dashed blue line, $g_j = g$) is plotted in Figs. 7(a) and 7(b). In this case the self-pulsing does not occur and the cavity photon number reaches a steady state at $\langle a^\dagger a \rangle = \Omega^2/4g^2$ very quickly. The steady-state value for the excited state population ($\langle \sigma^{22} \rangle \approx 1.7 \cdot 10^{-3}$) is reached much later. Note that the system with vanishing relative phase also reaches a steady state

with, surprisingly, the same photon number $\langle a^\dagger a \rangle = \Omega^2/4g^2$ but at a much higher excited state population ($\langle \sigma^{22} \rangle \approx 0.25$).

As we need an excited state population of at least 50% to observe the photon peaks, and the atoms perform Rabi oscillations to reach this, there should be a lower bound for the Rabi frequency Ω, depending on the laser-atom detuning δ_a, the atomic decay rate Γ, and the dephasing rate ν. This is exactly what we see in Fig. 7(c) and Fig. 7(d). The condition $\Omega > |\delta_a|$, $(\Gamma + \nu)/2$ needs to be satisfied in order for the peak intracavity photon number of the first pulse to appear. Furthermore, the collective photon emission from the atoms into the cavity is determined by the frequency $NC\Gamma$. Thus, for the superradiant photon pulse to dominate over the coherent drive, we need to ensure that $NC\Gamma > \Omega/2$. This threshold is also shown in Fig. 7(c) and Fig. 7(d).

VI. CONCLUSIONS

We have demonstrated and quantified the suppression of cavity superradiance of a noninverted atomic ensemble with an overall vanishing collective cavity coupling. With the representation of the collective atomic states in the Dicke basis we have introduced an intuitive picture for the system, which explains the number of emitted photons and the retained population after the superradiant emission. Compared to a longitudinal pump through the cavity, the transverse drive leads to an increased pulse delay time, which makes its measurement experimentally much more accessible. We have proposed a particular use case for the transition from cavity sub- to superradiance in the form of a cavity-enhanced Ramsey spectroscopy, which simplifies and accelerates the measurement procedure. We found that the chosen operating conditions with weak single atom coupling but strong collective coupling also induce an intriguing self-pulsing instability for continuous drive at suitable Rabi frequencies. Interestingly, the necessary operating conditions are within reach of current experimental setups [18,19,28].

Some preliminary investigations of the influence of imperfections in the setup as variable coupling strengths, slow atomic motion, or fluctuations in the excitation procedure qualitatively yield very similar results for experimentally realistic assumptions. However, a more detailed study of these
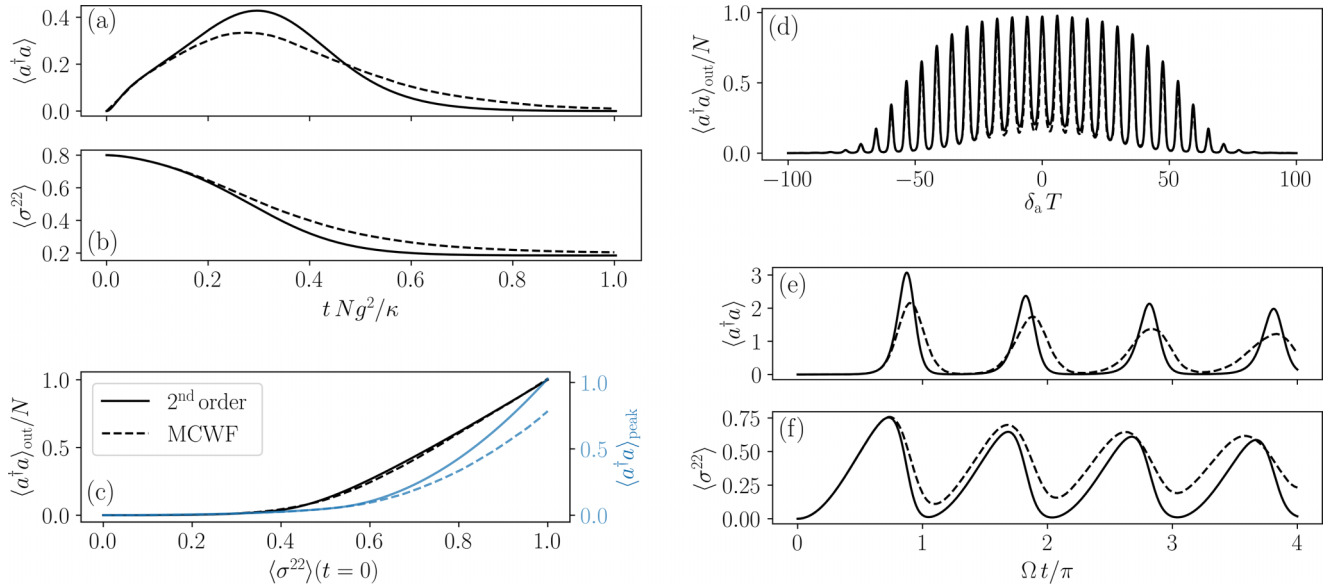
FIG. 8. Full Quantum Model. The second order cumulant expansion (solid line) is compared with a full quantum model (dashed line) for the cavity subradiance in (a)-(c), the cavity Ramsey method in (d) and the self-pulsing in (e) and (f). In all plots we used $\kappa = 200$, $\Gamma = \nu = 0$ and $\delta_c = \delta_a$. For (a)-(c) the remaining parameters are $N = 20$, $g = 10$ and $\delta_a = 0$, for (d) $N = 20$, $g = 10$, $\Omega = 100$ and $T = \pi/10$ and for (e)-(f) $N = 2 \cdot 50$, $g = 4$, $\delta_a = 0$ and $\Omega = 4$.

and other aspects such as heating and loss is required for a quantitative prediction of the practical system performance.

APPENDIX A: COMPARISON WITH FULL QUANTUM MODEL

To ensure the validity of our second-order cumulant expansion we compare the results with a full quantum model. Of course this is only possible for a relatively small number of atoms. To push the number of atoms as far as possible we use the Monte Carlo wave-function method [48–50], and describe the atoms in the Dicke basis which means that only collective atomic effects are captured. Thus, we neglect individual atomic decay and dephasing. Figure 8 shows the comparison between the second order cumulant expansion and the full quantum model for the cavity subradiance [Fig. 8(a)–8(c)], cavity Ramsey method [Fig. 8(d)] and self-pulsing [Fig 8(e)–8(f)]. Overall, we find a good qualitative agreement. A perfect quantitative correspondence is not to be expected for such small atom numbers. Note that the emitted photons we obtain in the time evolution of the full quantum treatment in Fig. 8(c) coincide with the ones calculated from the population distribution of the Dicke states as described in Sec. III A.
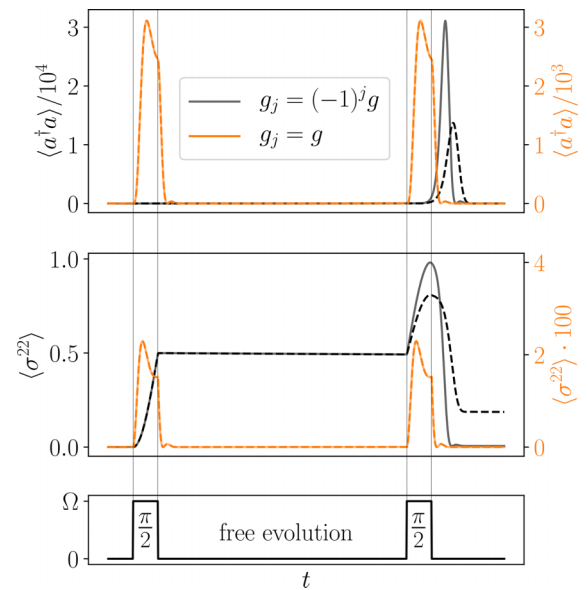

FIG. 9. Cavity Ramsey Sequence Time Evolution. For opposite phase coupling of two subensembles (black lines) the atomic population (middle graph) shows almost no decay between the two Ramsey $\pi/2$-pulses depicted in the lowest graph. A pulsed photon signal (upper graph) is obtained after the second pulse only. The maximum photon number appears in the resonant ($\delta_a = 0$, solid) case and becomes smaller for the detuned case ($\delta_a = 50\Gamma$, dashed). In contrast, for all atoms identically coupled (orange lines) cavity-induced superradiant decay creates an almost identical photon signal after each pulse virtually transferring all atoms to the ground state independent of their detuning. The parameters are chosen as in Fig. 6 except for the free evolution time between the two $\pi/2$-pulses, which we set to $T = \pi/200\Gamma$. The solid lines show $\delta_c = \delta_a = 0\Gamma$ and the dashed lines depict $\delta_c = \delta_a = 50\Gamma$.

APPENDIX B: DICKE STATE MAPPING

If we represent the collective state of identical two-level atoms in the Dicke state basis, the cavity-induced collective decay is only described by a vertical line, i.e., merely reducing M without changing J, if all atoms couple identically to the cavity. This is obviously not the case for our system. However, we can transform our system into a reference frame where the atoms have an alternating phase. This leads to an effective system with equal cavity coupling for all atoms, but a relative phase between atoms. This means for the preparation of the atoms with the coherent drive, that the phase of the Rabi frequency Ω is alternating, instead of the cavity coupling. To numerically calculate the correct state occupation for N atoms, as depicted in Fig. 4, we prepare

two spin-$N/4$ particles with coherent drives of opposite phase, and combine these two spins by, e.g., using Clebsch-Gordan coefficients.

APPENDIX C: CAVITY RAMSEY TIME EVOLUTION

Figure 9 shows a typical time evolution of the cavity Ramsey method for two different detunings $\delta_a = 0$ and $\delta_a = 50\Gamma$. The measured signal corresponds to the area below the curve of the photon number $\langle a^\dagger a \rangle$ times κ. Additionally, we plot the same quantities for the case of equally coupled atoms ($g_j = g$). We observe that a detuning of $\delta_a = 50\Gamma$ does not significantly change the time evolution and therefore also the signal (the solid and dashed orange lines overlap).

---

[1] R. H. Dicke, Coherence in spontaneous radiation processes, Phys. Rev. **93**, 99 (1954).

[2] R. H. Lehmberg, Radiation from an n-atom system. i. general formalism, Phys. Rev. A **2**, 883 (1970).

[3] M. Gross and S. Haroche, Superradiance: An essay on the theory of collective spontaneous emission, Phys. Rep. **93**, 301 (1982).

[4] Z. Ficek and R. Tanaś, Entangled states and collective nonclassical effects in two-atom systems, Phys. Rep. **372**, 369 (2002).

[5] S. Filipp, A. F. van Loo, M. Baur, L. Steffen, and A. Wallraff, Preparation of subradiant states using local qubit control in circuit qed, Phys. Rev. A **84**, 061805(R) (2011).

[6] R. Reimann, W. Alt, T. Kampschulte, T. Macha, L. Ratschbacher, N. Thau, S. Yoon, and D. Meschede, Cavity-Modified Collective Rayleigh Scattering of Two Atoms, Phys. Rev. Lett. **114**, 023601 (2015).

[7] B. Casabone, K. Friebe, B. Brandstätter, K. Schüppert, R. Blatt, and T. E. Northup, Enhanced Quantum Interface with Collective Ion-Cavity Coupling, Phys. Rev. Lett. **114**, 023602 (2015).

[8] M. A. Norcia, M. N. Winchester, J. R. K. Cline, and J. K. Thompson, Superradiance on the millihertz linewidth strontium clock transition, Sci. Adv. **2**, e1601231 (2016).

[9] L. Ostermann, C. Meignant, C. Genes, and H. Ritsch, Super-and subradiance of clock atoms in multimode optical waveguides, New J. Phys. **21**, 025004 (2019).

[10] A. Piñeiro Orioli, J. K. Thompson, and A. M. Rey, Emergent Dark States from Superradiant Dynamics in Multilevel Atoms in a Cavity, Phys. Rev. X **12**, 011054 (2022).

[11] D. F. Kornovan, N. V. Corzo, J. Laurat, and A. S. Sheremet, Extremely subradiant states in a periodic one-dimensional atomic array, Phys. Rev. A **100**, 063832 (2019).

[12] M. Moreno-Cardoner, R. Holzinger, and H. Ritsch, Efficient nano-photonic antennas based on dark states in quantum emitter rings, Opt. Express **30**, 10779 (2022).

[13] S. J. Masson, I. Ferrier-Barbut, L. A. Orozco, A. Browaeys, and A. Asenjo-Garcia, Many-Body Signatures of Collective Decay in Atomic Chains, Phys. Rev. Lett. **125**, 263601 (2020).

[14] A. Tiranov, V. Angelopoulou, C. J. van Diepen, B. Schrinski, O. A. D. Sandberg, Y. Wang, L. Midolo, S. Scholz, A. D. Wieck, A. Ludwig *et al.*, Coherent super-and subradiant dynamics between distant optical quantum emitters, arXiv:2210.02439 (2022).

[15] M. Zanner, T. Orell, C. M. Schneider, R. Albert, S. Oleschko, M. L. Juan, M. Silveri, and G. Kirchmair, Coherent control of a multi-qubit dark state in waveguide quantum electrodynamics, Nat. Phys. **18**, 538 (2022).

[16] S. Okaba, D. Yu, L. Vincetti, F. Benabid, and H. Katori, Superradiance from lattice-confined atoms inside hollow core fibre, Commun. Phys. **2**, 1 (2019).

[17] J. A. Mlynek, A. A. Abdumalikov, C. Eichler, and A. Wallraff, Observation of dicke superradiance for two artificial atoms in a cavity with high decay rate, Nat. Commun. **5**, 1 (2014).

[18] T. Laske, H. Winter, and A. Hemmerich, Pulse Delay Time Statistics in a Superradiant Laser with Calcium Atoms, Phys. Rev. Lett. **123**, 103601 (2019).

[19] S. A. Schäffer, M. Tang, M. R. Henriksen, A. A. Jørgensen, B. T. Christensen, and J. W. Thomsen, Lasing on a narrow transition in a cold thermal strontium ensemble, Phys. Rev. A **101**, 013819 (2020).

[20] M. Tang, S. A. Schäffer, A. A. Jørgensen, M. R. Henriksen, B. T. Christensen, J. H Müller, and J. W. Thomsen, Cavity-immune spectral features in the pulsed superradiant crossover regime, Phys. Rev. Res. **3**, 033258 (2021).

[21] F. Haake, M. I. Kolobov, C. Fabre, E. Giacobino, and S. Reynaud, Superradiant Laser, Phys. Rev. Lett. **71**, 995 (1993).

[22] D. Meiser, J. Ye, D. R. Carlson, and M. J. Holland, Prospects for a Millihertz-Linewidth Laser, Phys. Rev. Lett. **102**, 163601 (2009).

[23] J. G. Bohnet, Z. Chen, J. M. Weiner, D. Meiser, M. J. Holland, and J. K. Thompson, A steady-state superradiant laser with less than one intracavity photon, Nature (London) **484**, 78 (2012).

[24] H. Ritsch, P. Domokos, F. Brennecke, and T. Esslinger, Cold atoms in cavity-generated dynamical optical potentials, Rev. Mod. Phys. **85**, 553 (2013).

[25] W. Guerin, M. O. Araújo, and R. Kaiser, Subradiance in a Large Cloud of Cold Atoms, Phys. Rev. Lett. **116**, 083601 (2016).

[26] A. Shankar, J. T. Reilly, S. B. Jäger, and M. J. Holland, Subradiant-to-Subradiant Phase Transition in the Bad Cavity Laser, Phys. Rev. Lett. **127**, 073603 (2021).

[27] M. Gegg, A. Carmele, A. Knorr, and M. Richter, Superradiant to subradiant phase transition in the open system dicke model: Dark state cascades, New J. Phys. **20**, 013006 (2018).

[28] M. A. Norcia, J. R. K. Cline, J. A. Muniz, J. M. Robinson, R. B. Hutson, A. Goban, G. E. Marti, J. Ye, and J. K. Thompson,

Frequency Measurements of Superradiance from the Strontium Clock Transition, Phys. Rev. X **8**, 021036 (2018).

[29] L. Ostermann, H. Ritsch, and C. Genes, Protected State Enhanced Quantum Metrology with Interacting Two-Level Ensembles, Phys. Rev. Lett. **111**, 123601 (2013).

[30] L. Ostermann, D. Plankensteiner, H. Ritsch, and C. Genes, Protected subspace ramsey spectroscopy, Phys. Rev. A **90**, 053823 (2014).

[31] C. Gardiner, P. Zoller, and P. Zoller, *Quantum Noise: A Handbook of Markovian and Non-Markovian Quantum Stochastic Methods with Applications to Quantum Optics* (Springer Science & Business Media, New York, 2004).

[32] R. Kubo, Generalized cumulant expansion method, J. Phys. Soc. Jpn. **17**, 1100 (1962).

[33] D. Plankensteiner, C. Hotter, and H. Ritsch, QuantumCumulants.jl: A Julia framework for generalized mean-field equations in open quantum systems, Quantum **6**, 617 (2022).

[34] See Supplemental Material at http://link.aps.org/supplemental/10.1103/PhysRevResearch.5.013056 for a Julia code example to derive and numerically solve the equations for our system.

[35] N. Shammah, S. Ahmed, N. Lambert, S. De Liberato, and F. Nori, Open quantum systems with local and collective incoherent processes: Efficient numerical simulations using permutational invariance, Phys. Rev. A **98**, 063815 (2018).

[36] Y. Zhang, Y.-X. Zhang, and K. Mølmer, Monte-carlo simulations of superradiant lasing, New J. Phys. **20**, 112001 (2018).

[37] D. Ferraro, M. Campisi, G. M. Andolina, V. Pellegrini, and M. Polini, High-Power Collective Charging of a Solid-State Quantum Battery, Phys. Rev. Lett. **120**, 117702 (2018).

[38] F. Pirmoradian and K. Mølmer, Aging of a quantum battery, Phys. Rev. A **100**, 043833 (2019).

[39] G. Ferioli, A. Glicenstein, L. Henriet, I. Ferrier-Barbut, and A. Browaeys, Storage and Release of Subradiant Excitations in a Dense Atomic Cloud, Phys. Rev. X **11**, 021031 (2021).

[40] H. Liu, S. B. Jäger, X. Yu, S. Touzard, A. Shankar, M. J. Holland, and T. L. Nicholson, Rugged mHz-Linewidth Superradiant Laser Driven by a Hot Atomic Beam, Phys. Rev. Lett. **125**, 253602 (2020).

[41] J. Kim, S.-h. Oh, D. Yang, J. Kim, M. Lee, and K. An, A photonic quantum engine driven by superradiance, Nat. Photonics **16**, 707 (2022).

[42] J. Lodewyck, P. G. Westergaard, and P. Lemonde, Nondestructive measurement of the transition probability in a sr optical lattice clock, Phys. Rev. A **79**, 061401(R) (2009).

[43] G. Vallet, E. Bookjans, U. Eismann, S. Bilicki, R. Le Targat, and J. Lodewyck, A noise-immune cavity-assisted non-destructive detection for an optical lattice clock in the quantum regime, New J. Phys. **19**, 083002 (2017).

[44] R. Hobson, W. Bowden, A. Vianello, I. R. Hill, and P. Gill, Cavity-enhanced non-destructive detection of atoms for an optical lattice clock, Opt. Express **27**, 37099 (2019).

[45] N. F. Ramsey, A molecular beam resonance method with separated oscillating fields, Phys. Rev. **78**, 695 (1950).

[46] Y. Sortais, S. Bize, M. Abgrall, S. Zhang, C. Nicolas, C. Mandache, P. Lemonde, P. Laurent, G. Santarelli, N. Dimarcq *et al.*, Cold atom clocks, Phys. Scr. **2001**, 50 (2001).

[47] S. Bize, P. Laurent, M. Abgrall, H. Marion, I. Maksimovic, L. Cacciapuoti, J. Grünert, C. Vian, F. P. Dos Santos, P. Rosenbusch *et al.*, Cold atom clocks and applications, J. Phys. B: At., Mol. Opt. Phys. **38**, S449 (2005).

[48] S. Krämer, D. Plankensteiner, L. Ostermann, and H. Ritsch, Quantumoptics.jl: A Julia framework for simulating open quantum systems, Comput. Phys. Commun. **227**, 109 (2018).

[49] R. Dum, P. Zoller, and H. Ritsch, Monte carlo simulation of the atomic master equation for spontaneous emission, Phys. Rev. A **45**, 4879 (1992).

[50] K. Mølmer, Y. Castin, and J. Dalibard, Monte carlo wave-function method in quantum optics, J. Opt. Soc. Am. B **10**, 524 (1993).